COMBINED IN-PLANE AND THROUGH-THE-THICKNESS ANALYSIS FOR FAILURE PREDICTION OF BOLTED COMPOSITE JOINTS

V. Kradinov,[*] E. Madenci[†]
The University of Arizona, Tucson, Arizona, 85715

D. R. Ambur[‡]
NASA Langley Research Center, Hampton, Virginia, 23681

Abstract

Although two-dimensional methods provide accurate predictions of contact stresses and bolt load distribution in bolted composite joints with multiple bolts, they fail to capture the effect of thickness on the strength prediction. Typically, the plies close to the interface of laminates are expected to be the most highly loaded, due to bolt deformation, and they are usually the first to fail. This study presents an analysis method to account for the variation of stresses in the thickness direction by augmenting a two-dimensional analysis with a one-dimensional through the thickness analysis. The two-dimensional in-plane solution method based on the combined complex potential and variational formulation satisfies the equilibrium equations exactly, and satisfies the boundary conditions and constraints by minimizing the total potential. Under general loading conditions, this method addresses multiple bolt configurations without requiring symmetry conditions while accounting for the contact phenomenon and the interaction among the bolts explicitly. The through-the-thickness analysis is based on the model utilizing a beam on an elastic foundation. The bolt, represented as a short beam while accounting for bending and shear deformations, rests on springs, where the spring coefficients represent the resistance of the composite laminate to bolt deformation. The combined in-plane and through-the-thickness analysis produces the bolt/hole displacement in the thickness direction, as well as the stress state in each ply. The initial ply failure predicted by applying the average stress criterion is followed by a simple progressive failure. Application of the model is demonstrated by considering single- and double-lap joints of metal plates bolted to composite laminates.

---

*Technical Expert, Department of Aerospace and Mechanical Engineering.

†Professor, Department of Aerospace and Mechanical Engineering. Member AIAA.

‡Head, Mechanics and Durability Branch. Associate Fellow AIAA.

Introduction

Bolts provide the primary means of connecting composite parts in the construction of aircraft and aerospace vehicles. The main disadvantage of bolted joints is the formation of high stress concentration zones at the locations of bolt holes, which might lead to a premature failure of the joint due to net-section, shear-out, or bearing failures, or their combinations. The stress state in a bolted joint is dependent on the loading conditions, dimensions, laminate stacking sequence, bolt clamp-up forces, bolt location, bolt flexibility, bolt size, and bolt-hole clearance (or interference). A substantial number of experimental, analytical, and numerical investigations have been conducted on the stress analysis of bolted laminates. The study by Kradinov et al.[1] provides an extensive and detailed discussion of earlier investigations. In order to eliminate the shortcomings of the previous analyses, Kradinov et al. introduced a two-dimensional numerical/analytical method to determine the bolt load distribution in bolted single- and double-lap composite joints utilizing the complex potential-variational formulation. This method addresses multiple bolt configurations without requiring symmetry conditions while accounting for the contact phenomenon and the interaction among the bolts explicitly under bearing and by-pass loading. The contact stresses and contact regions are determined through an iterative procedure as part of the solution method.

Although this two-dimensional approach provides an accurate prediction of the contact stresses and bolt load distribution, it fails to capture the effect of thickness on the failure prediction. In addition to the head and nut shapes and the applied bolt torque, the stacking sequence considerably influences the stress state in each ply of the laminate. Thus, an adequate representation of the ply load variation through the thickness is critical for the failure prediction of composite laminates at the bolt-hole boundary.

This study presents an analysis method to account for the variation of stresses in the thickness direction by augmenting the two-dimensional analysis by Kradinov et al.[1] with a model of a bolt on an elastic foundation, as suggested by Ramkumar et al.[2] The bolt, represented as a beam while accounting for bending and shear deformations, rests on springs, where the spring coefficients

represent the resistance of the composite laminate to bolt deformations. The values of the spring coefficients depend on the fiber orientation of the laminate plies; for isotropic plates, the spring coefficients are defined by a constant value. The present analysis produces the bolt/hole displacement in the thickness direction and the stress state in each ply. Failure load and associated failure modes of net-section, bearing, and shear-out for composite bolted joints are predicted based on the average stress criterion of Whitney and Nuismer[3] for first ply failure, followed by a simple progressive failure criterion as suggested by Ramkumar et al.[2]

The applicability of this method is demonstrated by considering single- and double-lap joints of laminates with a varying number of bolts. In addition to the determination of the contact stresses and the bolt load distributions, the failure load is investigated by applying a progressive failure procedure based on the average stress failure criterion.

Problem Statement

The geometry of bolted single- and double-lap joints of composite laminates is described in Fig. 1. Each joint can be subjected to a combination of bearing, by-pass, and shear loads. Each laminate of the single- and double-lap joints, joined with L number of bolts, can be subjected to tractions and displacement constraints along its external boundary. The thickness of the laminates is denoted by h_k. As illustrated in Fig. 2, the hole radius in the k^{th} laminate associated with the ℓ^{th} bolt, $a_{k,\ell}$ (which is slightly larger than the bolt radius, R_ℓ), leads to a clearance of $\delta_{k,\ell}$. The ranges of the subscripts are specified by $k = 1,...,K$ and $\ell = 1,...,L$, with K and L being the total number of laminates and bolts, respectively. The bolt radius remains the same in each laminate; however, the radii of the holes associated with the same bolt are not necessarily the same.

The extent of the contact region is dependent on the bolt displacement deformation of the hole boundary, and the clearance. The presence of friction between the bolts and the laminates is disregarded. Each laminate with a symmetric lay-up of N_k plies can have distinct anisotropic material properties. Each bolt can also have a distinct stiffness, and the explicit expressions for bolt stiffness for a single- and double-lap joint, as well as the general lap configurations, are derived in Kradinov et al.[1]

The problem posed concerns the determination of the extent of the contact zones, the contact stresses and the bolt load distribution under general loading conditions, the bolt/hole deformation, and the stress state in each ply, and thus the joint strength.

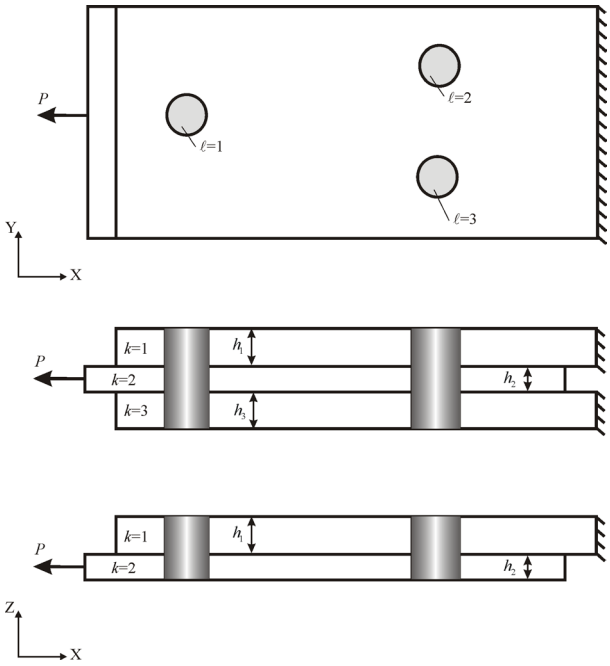

Fig. 1 Geometric description of single- and double-lap bolted joints.

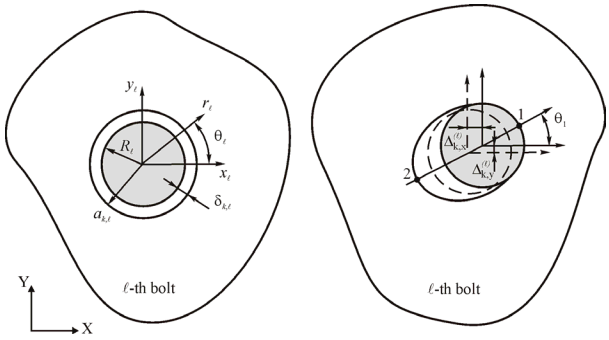

Fig. 2 Position of a bolt before and after the load is exerted.

Solution Method

In-Plane Analysis for Contact Stresses and Bolt Load Distribution

The coupled complex potential and variational formulation introduced by Kradinov et al.[1,4] is employed to determine the two-dimensional stress and strain fields required for the computation of the contact stresses and contact regions, as well as the bolt load distribution. This in-plane analysis is capable of accounting for finite laminate planform dimensions, uniform and variable laminate thickness, laminate lay-up, interaction among bolts, bolt torque, bolt flexibility, bolt size, bolt-hole clearance and interference, insert dimensions, and insert material properties. Unlike the finite

element method, it alleviates the extensive and expensive computations arising from the non-linear nature of the contact phenomenon. Also, the method is more suitable for parametric study and design optimization.

Although this two-dimensional analysis provides accurate in-plane stresses in each laminate and bolt load distribution, it assumes no variation of stresses through the laminate thickness. This assumption might lead to erroneous results in the strength prediction of bolted joints because of the pronounced influence of through-the-thickness stress variation at the bolt location as discussed by Ramkumar et al.[2]

Through-Thickness Analysis for Bolt/Hole Deformation

In conjunction with a two-dimensional in-plane bolted joint analysis, Ramkumar et al.[2] suggested a model utilizing a beam on an elastic foundation in order to include the variation of stresses in the thickness direction of the bolted joint. The bolt rests on springs, where the spring constants represent the resistance of the laminate to bolt deformation. The spring constants correspond to the modulus of each ply through the thickness of the hole boundary. Their values depend on the ply orientation of the laminate. For isotropic plates, the spring constants have a uniform value.

As the bolt bends, the plies are loaded differently near the hole boundary based on their orientation and location. As shown in Fig. 3, the plies close to the interface of adjacent laminates exhibit significant deformation. As shown in Fig. 4, the beam representing the bolt rests on an elastic foundation whose modulus is represented by the stiffness of each ply, $k_{k,i}^{(\ell)}$, in the laminate. The superscript ℓ and subscripts k and i denote the specific bolt, the laminate, and the ply numbers, respectively. Also, the bolt is subjected to constraints at the head and nut locations through rotational stiffness constants, $k_h^{(\ell)}$ and $k_n^{(\ell)}$, in order to include the effect of head and nut shapes and bolt torque.

Free-body diagrams of the laminates at the ℓ^{th} bolt in a single- and double-lap joint and the end conditions and slope continuity conditions in the presence of both bending and shear deformations are shown in Fig. 5. In accordance with the typical bolt deformation illustrated in Fig. 3, the force exerted by the ℓ^{th} bolt on the k^{th} laminate, $P_k^{(\ell)}$ (obtained from the two-dimensional in-plane analysis), is enforced as a shear force, $V_k^{(\ell)}$, at the interface of the adjacent laminates. At the interface, the continuity of the bending slopes, $\psi_k^{(\ell)} = \psi_{k+1}^{(\ell)}$, is also enforced while permitting the laminates to displace. At the head and nut locations of the bolt, the shear force values are set to zero, and the rotations (slopes) are dictated by rotational stiffness constants, $k_h^{(\ell)}$ and $k_n^{(\ell)}$, depending on the bolt type, presence of washers, and the applied bolt torque.

Finite Element Analysis. The bolt/hole displacements through the laminate thickness are obtained by discretizing the bolt with beam elements that account for bending and shear deformations. The bolt discretization is based on the discrete nature of the ply stacking sequence. Along its thickness, each ply is discretized with two beam elements. For both single- and double-lap joints, the number of elements and the number of nodes in relation to the number of plies in the laminate are described in Fig. 6. In the discretization process, a node located in the middle of each ply is attached to a spring element representing the ply stiffness (Fig. 6).

The derivation of the stiffness matrix composed of a two-noded beam element (Timoshenko's zeroth-order shear deformable beam theory) and a linear spring element is presented in the Appendix.

Associated with the k^{th} laminate and the ℓ^{th} bolt, each node is assigned a deflection, $\Delta_{k,j}^{(\ell)} = \Delta_k^{(\ell)}(z_j)$, and a rotation, $\phi_{k,j}^{(\ell)} = \phi_k^{(\ell)}(z_j)$, with the subscript j representing the node number. In the finite element formulation, the rotations of the internal nodes are statically condensed in terms of the nodal displacements and the end node rotations. The positive directions of the deflections and rotations are shown in Fig. 7. The details of the condensation procedure are also explained in the Appendix.

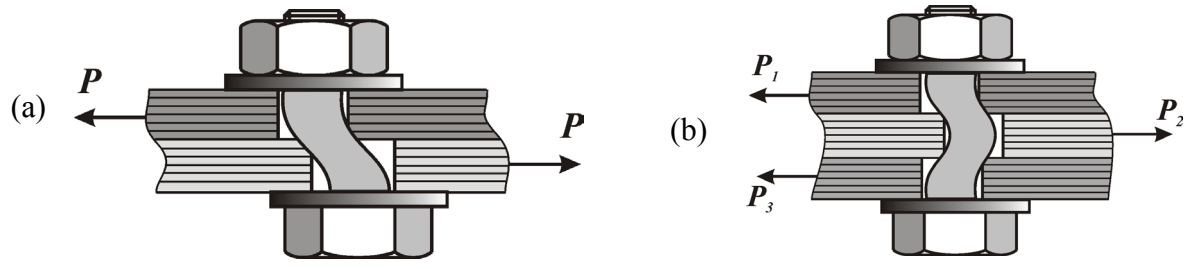

Fig. 3 Typical bolt deformation in a (a) single- and (b) double-lap joint.

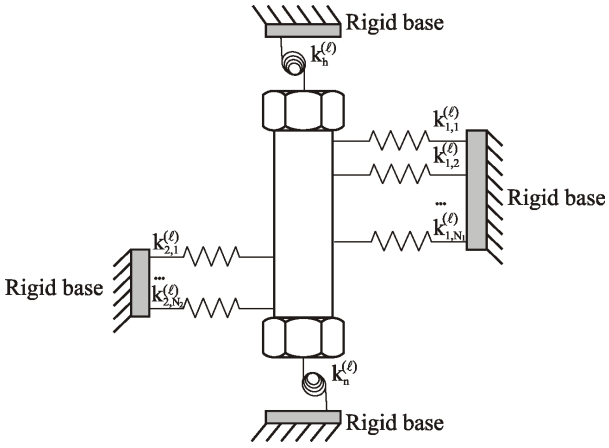

(a)

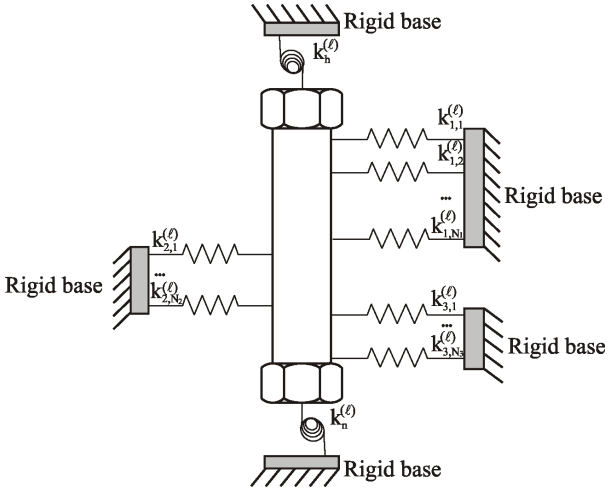

(b)

Fig. 4 Bolt on an elastic foundation model in a (a) single- and (b) double-lap joint.

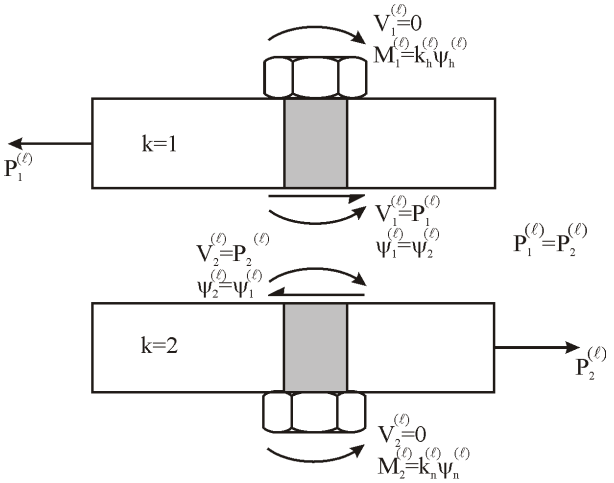

(a)

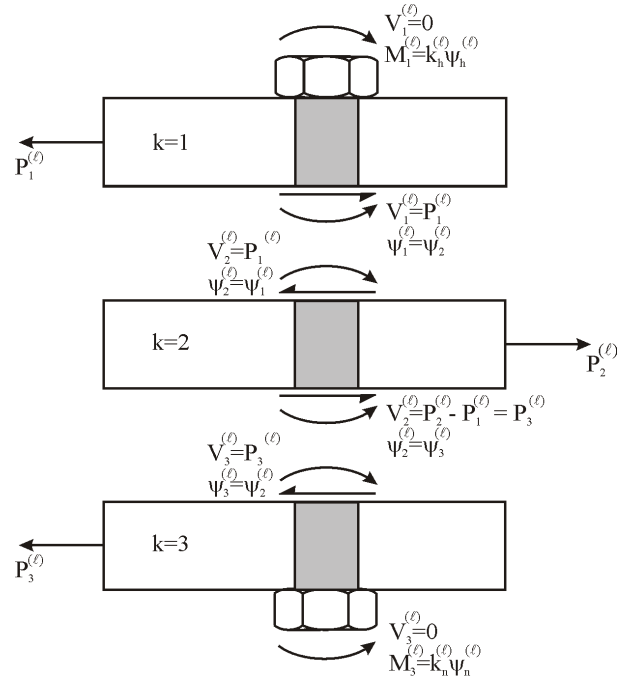

(b)

Fig. 5 Free-body diagrams of laminates for a (a) single- and (b) double-lap joint.

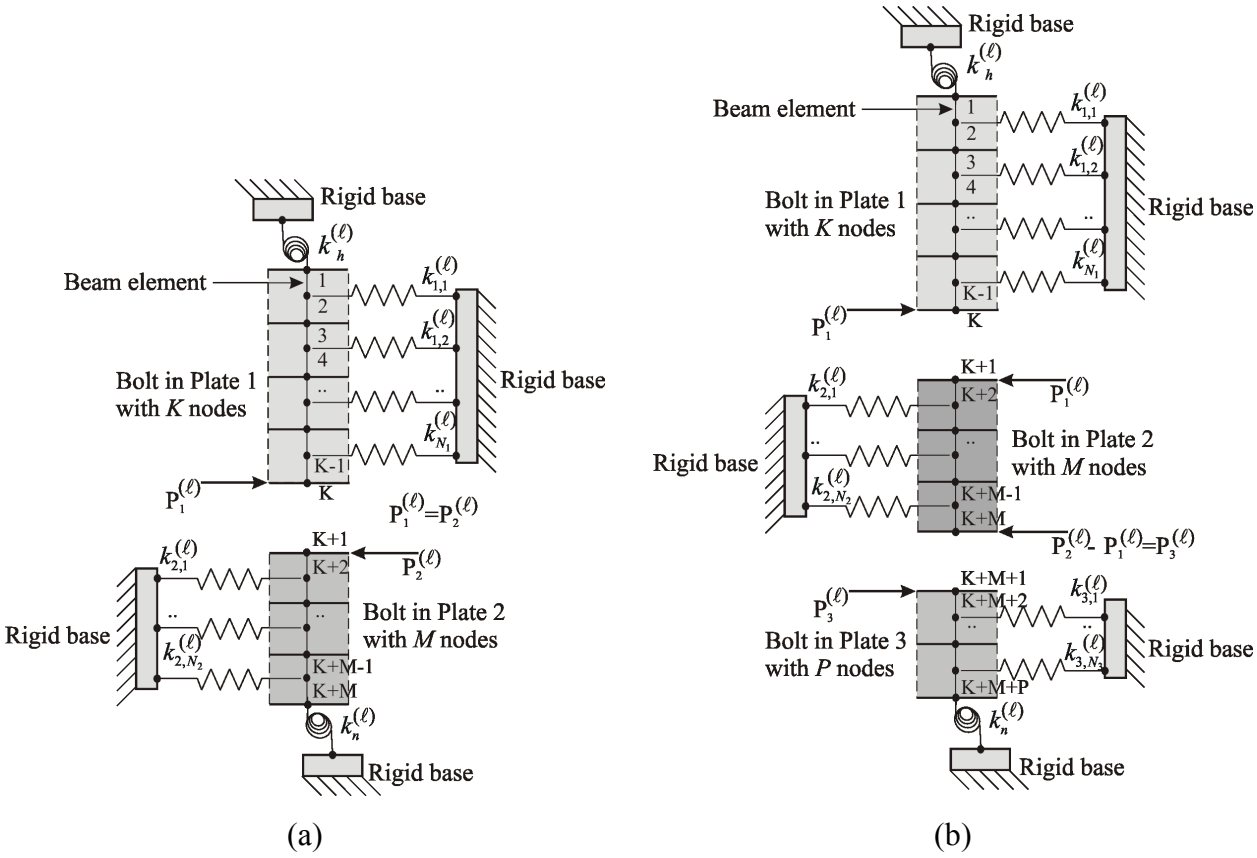

Fig. 6 The finite element model of a bolt in a (a) single-and (b) double-lap joint.

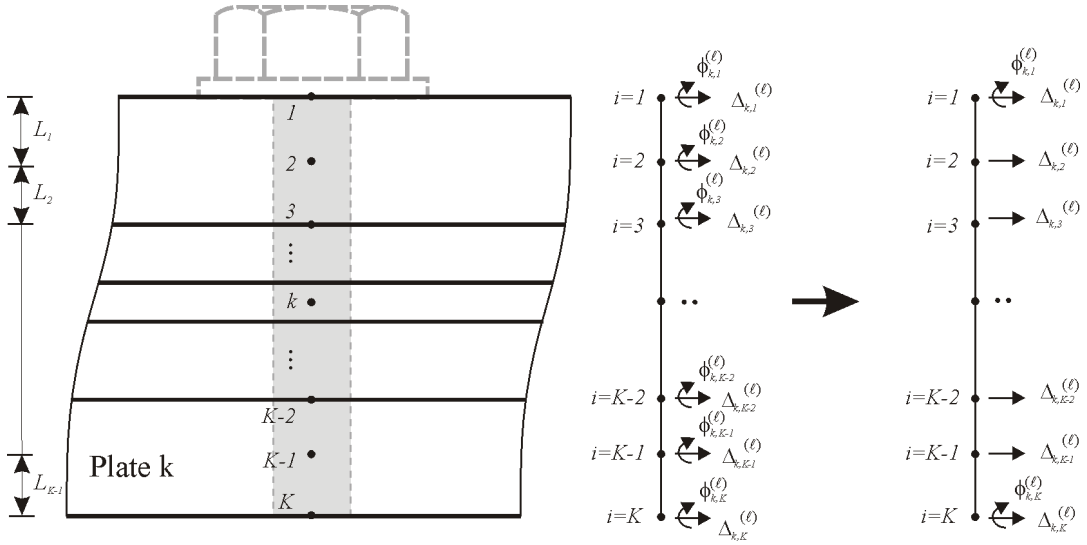

Fig. 7 Bolt discretization in the k^{th} plate after static condensation.

Spring Stiffness Coefficients. As suggested by Ramkumar et al.[2], the translational spring stiffness coefficients, $k_{k,i}^{(\ell)}$, representing the i^{th} ply of the k^{th} laminate near the ℓ^{th} bolt are approximated by

$$k_{k,i}^{(\ell)} = \frac{P_{k,i}^{(\ell)}}{\gamma_k^{(\ell)}} \quad , \qquad i = 1, N_k \qquad (1)$$

where $p_{k,i}^{(\ell)}$ is the load exerted by the ℓ^{th} bolt on the i^{th} ply of the k^{th} laminate and $\gamma_k^{(\ell)}$ represents the maximum hole enlargement of the ℓ^{th} hole in the k^{th} laminate. The number of plies in the k^{th} laminate is denoted by N_k.

As part of the two-dimensional in-plane bolted joint analysis, the load exerted by the bolt on the i^{th} ply of the k^{th} laminate near the ℓ^{th} hole, $p_{k,i}^{(\ell)}$, is computed as

$$p_{k,i}^{(\ell)} = \sqrt{\left(p_{(k,i)x}^{(\ell)}\right)^2 + \left(p_{(k,i)y}^{(\ell)}\right)^2} \qquad (2)$$

where $p_{(k,i)x}^{(\ell)}$ and $p_{(k,i)y}^{(\ell)}$ represent its components in the *x*- and *y*-directions. These components are computed by integrating the radial stresses in each ply as

$$p_{(k,i)x}^{(\ell)} = a_{k,\ell} \int_0^{2\pi} \sigma_{rr}^{(k,i)}(r = a_{k,\ell}, \theta) \cos\theta \; d\theta \qquad (3a)$$

and

$$p_{(k,i)y}^{(\ell)} = a_{k,\ell} \int_0^{2\pi} \sigma_{rr}^{(k,i)}(r = a_{k,\ell}, \theta) \sin\theta \; d\theta \qquad (3b)$$

in which $a_{k,\ell}$ is the radius of the ℓ^{th} hole in the k^{th} laminate, and $\sigma_{rr}^{(k,i)}(r = a_{k,\ell}, \theta)$ represents the radial stress distribution in the i^{th} ply of the k^{th} laminate near the ℓ^{th} hole.

Under plane-stress assumptions, the stress and strain components are related by

$$\boldsymbol{\sigma}^{(k,i)} = \bar{\boldsymbol{Q}}_{k,i} \, \boldsymbol{\varepsilon}^{(k)} \qquad (4)$$

in which $\bar{\boldsymbol{Q}}_{k,i}$ represents the reduced stiffness matrix for the i^{th} ply of the k^{th} laminate. The Cartesian stress components in the i^{th} ply of the k^{th} laminate and the Cartesian strain components, uniform through the thickness of the k^{th} laminate, are included in the vectors of $\boldsymbol{\sigma}^{(k,i)}$ and $\boldsymbol{\varepsilon}^{(k)}$. This stress state in each ply is employed in the prediction of the initial ply failure load, $F_{k,i}^{(\ell)IN}$, and the corresponding failure mode.

As shown in Fig. 2, the maximum hole enlargement, $\gamma_k^{(\ell)}$, is defined as the absolute value of the difference between the radial displacements, $u_k^{(\ell)}(r = a_{k,\ell}, \theta = \theta_1)$ and $u_k^{(\ell)}(r = a_{k,\ell}, \theta = \theta_2)$,of points 1 and 2 on the hole boundary in the direction of the bolt load

$$\gamma_k^{(\ell)} = \left| u_k^{(\ell)}(r = a_{k,\ell}, \theta = \theta_2) - u_k^{(\ell)}(r = a_{k,\ell}, \theta = \theta_1) \right| \qquad (5)$$

where the radial displacements are obtained from the in-plane bolted joint analysis. The maximum hole-enlargement, $\gamma_k^{(\ell)}$, can be different for each laminate of the bolted joint, but is uniform through the thickness. Also, it is specific to each bolt-hole in the laminate because it is dependent on the deformation response and the bolt load distribution. The head and nut rotational stiffness coefficients, $k_h^{(\ell)}$ and $k_n^{(\ell)}$, respectively, have values close to zero for free-end conditions and to infinity for protruding head bolts under high torque. The stiffness matrix becomes singular if these coefficients approach zero.

The analysis results include displacements and rotations, $\Delta_{k,j}^{(\ell)}$ and $\phi_{k,j}^{(\ell)}$, at the j^{th} node, as well as the spring forces, $f_{k,i}^{(\ell)}$, at the i^{th} ply of the k^{th} laminate near the ℓ^{th} hole. The effect of through-the-thickness variation is invoked in the in-plane stress analysis by considering the spring forces, $f_{k,i}^{(\ell)}$, as the *corrected ply loads*.

Progressive Failure Prediction

There are three major failure modes in bolted composite lap joints: net-section, shear-out, and bearing (Fig. 8). The net-section failure is associated with fiber and matrix tension failure and shear-out and bearing failures are associated with fiber and matrix shear and compression failures, respectively. Failure in bolted laminates can be predicted by evaluating either the specific stress components or their interaction at characteristic distances from the hole boundary. Although any one of these criteria is applicable to the prediction of the failure of a laminate or a ply, values of the characteristic distances and the unnotched strength parameters of the material are scarce.

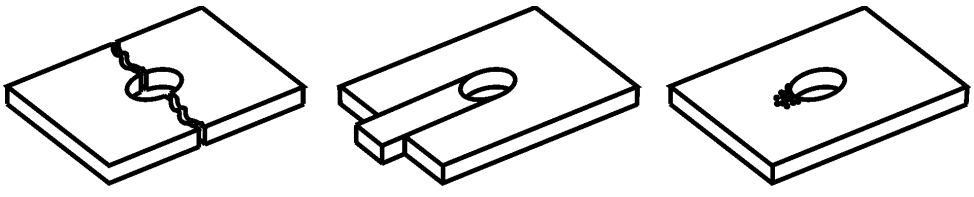

Fig. 8 Primary failure modes in bolted composite joints.

The point and average stress criteria introduced by Whitney and Nuismer[3] disregarded the interaction among the stress components. However, they are widely used in engineering practice for predicting the failure stress and failure modes because of their well-established values of the characteristic distances.[2,5,-6] Both of these criteria predict net-section, shear-out, and bearing failures when the stress components at specific locations reach their corresponding unnotched strength levels. The characteristic distances of a_o^{ns} for net-section, a_o^{br} for bearing, and a_o^{so} for shear-out failures, as well as the shear-out and net-section planes (denoted by the n and s lines), are shown in Fig. 9. According to the point stress criterion, the net-section failure occurs when the normal stress, σ_{ss}, at a distance a_o^{ns} from the bolt-hole boundary along the net-section plane reaches the unnotched tensile strength of a ply, X_t. If σ_{ss} at a distance a_o^{br} from the bolt hole boundary reaches the unnotched compressive strength of a ply, X_c, bearing failure occurs. Shear-out failure occurs when the shear stress, σ_{ns}, at a distance a_o^{so} from the bolt-hole boundary along the shear-out planes reaches the unnotched shear strength of a ply, X_s. The average stress failure criterion is based on the average values of the corresponding stress components over the characteristic distances of $(0, a_0^{ns})$, $(0, a_0^{br})$, and $(0, a_0^{so})$.

Under the specified external loading, the ratios $C_{j,i}^{(k,\ell)}$ $(j = ns, br, so)$ of the unnotched strength parameters to the average stresses associated with the net-section $(j = ns)$, bearing $(j = br)$, and shear-out $(j = so)$ failure modes at the i^{th} ply of the k^{th} laminate near the ℓ^{th} hole are defined in the form

$$C_{ns,i}^{(k,\ell)} = \frac{X_t^{(k,i)}}{\bar{\sigma}_{ss}^{(k,i)}} \text{ for net-section failure mode} \qquad (6a)$$

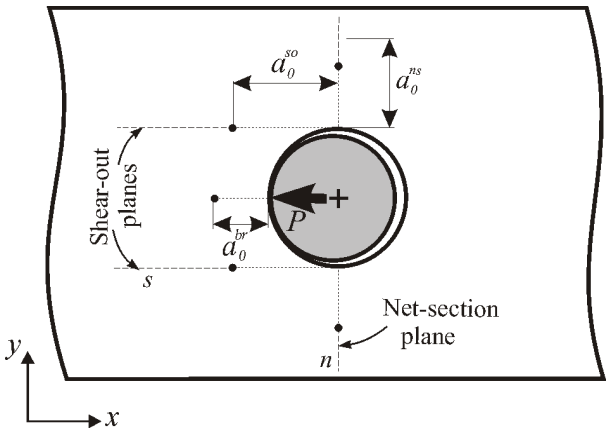

Fig. 9 Characteristic distances for point and average stress failure criteria.

$$C_{br,i}^{(k,\ell)} = \frac{X_c^{(k,i)}}{\bar{\sigma}_{ss}^{(k,i)}} \text{ for bearing failure mode} \qquad (6b)$$

$$C_{so,i}^{(k,\ell)} = \frac{X_s^{(k,i)}}{\bar{\sigma}_{ns}^{(k,i)}} \text{ for shear-out failure mode} \qquad (6c)$$

in which $\bar{\sigma}_{ss}^{(k,i)}$ and $\bar{\sigma}_{ns}^{(k,i)}$ are averaged normal and shear stresses over the characteristic distances $(0, a_0^{ns})$, $(0, a_0^{br})$, and $(0, a_0^{so})$.

The initial ply failure load, $F_{k,i}^{(\ell)IN}$, and its associated failure mode are established by

$$F_{k,i}^{(\ell)IN} = \min\left(C_{j,i}^{(k,\ell)}\right) p_{k,i}^{(\ell)}, \qquad \left(j = ns, br, so\right) \qquad (7)$$

After the initial failure, a ply is assumed to continue sustaining the applied load according to a bilinear behavior, shown in Fig. 10. The value of the ultimate ply failure load, $F_{k,i}^{(\ell)UL}$, is defined by

$$F_{k,i}^{(\ell)UL} = HF_{k,i}^{(\ell)IN} \qquad (8)$$

where the factor H varies as 1.02, 1.50, and 1.12 for net-section, bearing, and shear-out failure modes, respectively, as suggested by Ramkumar et al.[2]

Due to the bilinear ply load behavior, the applied joint load is increased incrementally while predicting ply failure subsequent to the initial ply failure. At each load increment, the corrected ply loads, $f_{k,i}^{(\ell)}$, are compared to the initial and ultimate ply failure loads of $F_{k,i}^{(\ell)IN}$ and $F_{k,i}^{(\ell)UL}$, which are predicted according to the average stress criterion of two-dimensional analysis.

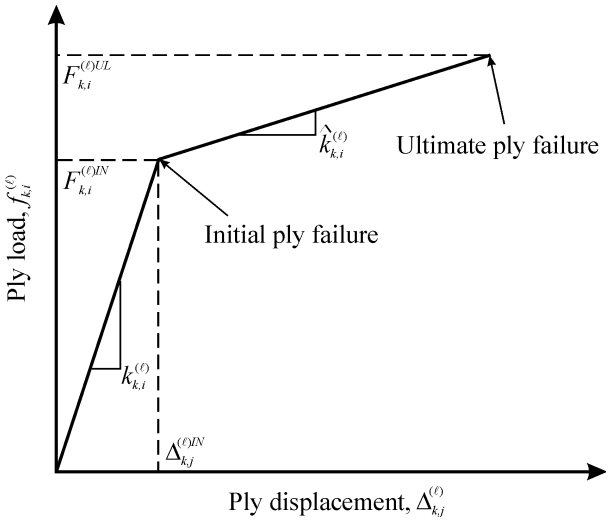

Fig. 10 Bilinear ply behavior.

For an *undamaged* ply, if the corrected ply load of $f_{k,i}^{(\ell)}$ exceeds the corresponding initial ply failure load of $F_{k,i}^{(\ell)IN}$, the ply experiences initial failure. Accordingly, as suggested by Ramkumar et al.,[2] the initial ply stiffness of $k_{k,i}^{(\ell)}$ is reduced to $\hat{k}_{k,i}^{(\ell)}$. The reduced ply stiffness, $\hat{k}_{k,i}^{(\ell)}$, is defined by

$$\hat{k}_{k,i}^{(\ell)} = \alpha\, k_{k,i}^{(\ell)} \tag{9}$$

in which the parameter α is assumed to be 0.1. For a *damaged* ply, if the corrected ply load of $f_{k,i}^{(\ell)}$ exceeds the corresponding ultimate failure load of $F_{k,i}^{(\ell)UL}$, the ply experiences total failure. Consequently, the ply stiffness is reduced to zero.

Based on the bilinear behavior of the ply load shown in Fig. 10, the ply load at the i^{th} ply of the k^{th} laminate near the ℓ^{th} bolt can be expressed in terms of the ply displacement as

$$f_{k,i}^{(\ell)} = k_{k,i}^{(\ell)} \Delta_{k,j}^{(\ell)} \tag{10a}$$

for an undamaged ply, as

$$f_{k,i}^{(\ell)} = \left(k_{k,i}^{(\ell)} - \hat{k}_{k,i}^{(\ell)}\right)\Delta_{k,j}^{(\ell)IN} + \hat{k}_{k,i}^{(\ell)} \Delta_{k,j}^{(\ell)} \tag{10b}$$

for a damaged ply, and as

$$f_{k,i}^{(\ell)} = 0 \tag{10c}$$

for a totally damaged ply, where j denotes the node associated with the translational spring element representing the i^{th} ply.

When a ply fails, the adjacent plies share the load released by the failed ply. Thus, the failure propagates from ply to ply until the total failure of the laminate. The ultimate joint failure load is defined as the joint load that results in the ultimate failure of half of the plies at a particular bolt location. The minimum of the failure loads predicted for each bolt establishes the strength of the joint. This type of progressive failure analysis can be employed in conjunction with any one of the available failure criteria.

Numerical Results

The capability of this combined in-plane and through-the-thickness bolted joint analysis is demonstrated by considering single- and double-lap bolted joints joining metal to composite laminates with one, three, and four bolts as shown in Figs. 11-13.

The material properties, stacking sequence and thickness of the plates are the same as those considered by

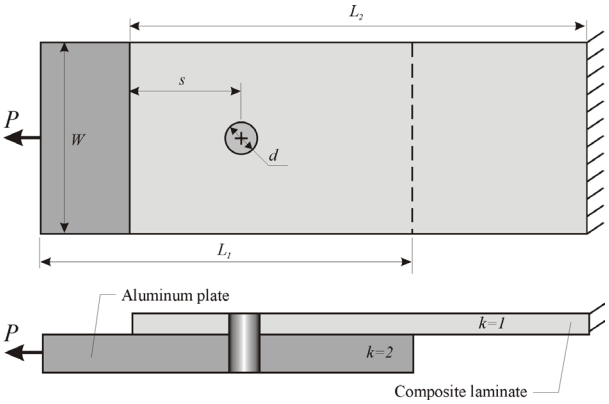

Fig. 11 One-bolt single-lap joint geometry and loading.

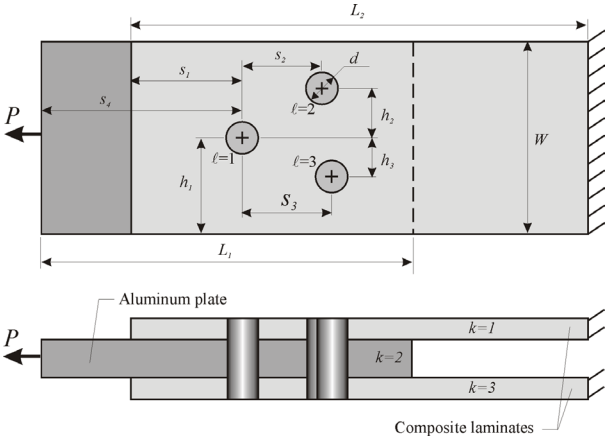

Fig. 12 Three-bolt double-lap joint geometry and loading.

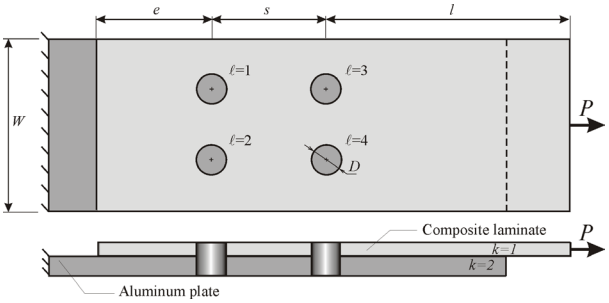

Fig. 13 Four-bolt single-lap joint geometry and loading.

Ramkumar et al.[2] The metal plates are made of aluminum with Young's modulus $E_a = 10.1$ Msi and Poisson's ratio $\nu_a = 0.3$. The bolts are of steel with a Young's modulus $E_s = 30.0$ Msi and Poisson's ratio $\nu_s = 0.3$. Although not a limitation of the analysis method, in these configurations, the bolt and hole diameters are equal, leading to zero clearance. The aluminum plates have a thickness of 0.31 in. The thickness of the laminate is 0.12 in with stacking sequence of $[(45°/0°/-45°/0°)_2 0°/90°]_s$. The material properties for each ply are specified as $E_L = 18.5$ Msi, $E_T = 1.9$ Msi, $G_{LT} = 0.85$ Msi, and $\nu_{LT} = 0.3$. The high value of torque applied on the protruding bolt-head is specified by the head and nut rotational stiffness coefficients of $k_h = 10^{12}$ lbs-in and $k_n = 10^{12}$ lbs-in. The failure prediction is performed by employing the average stress criterion along with a bilinear stiffness reduction after the initial failure of each ply. The characteristic length parameters for the average stress failure criterion are taken as a_0^{ns} =0.1 in, a_0^{so} =0.08 in, and a_0^{br} =0.025 in. The unnotched strength parameters of the ply for each orientation in the stacking sequence are given in Table 1.

Table 1 Unnotched strength values in *X*-direction.

Ply orientation (degree)	X_t, Net-section tensile (ksi)	X_c, Bearing (ksi)	X_s, Shear-out (ksi)
0	230.0	320.0	17.3
45	40.0	56.0	95.0
-45	40.0	56.0	95.0
90	9.5	38.9	17.3

As part of the finite element modeling, the section of the bolt in contact with the composite laminate is discretized with 41 nodes in order to represent 20 plies of the laminate lay-up. Because the aluminum plate is thicker than the laminate, it is discretized with 81 nodes leading to 40 layers of aluminum.

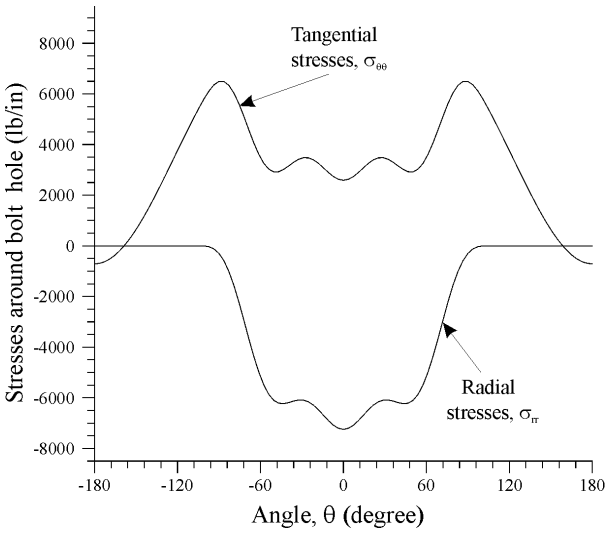

Fig. 14 Stress variation around the hole boundary in an aluminum plate.

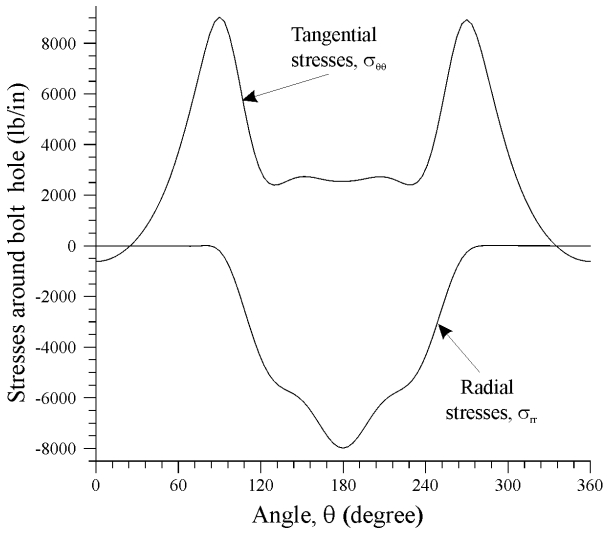

Fig. 15 Stress variation around the hole boundary in a composite laminate.

<u>One-Bolt Single-Lap Metal to Composite Joint</u>

The geometrical parameters shown in Fig. 11 are defined by W =1.875 in, d =0.3125 in, L_1 =3.6 in, L_2 =4.4375 in, and s =0.9375 in. The initial applied load of $P = 1875$ lbs is uniformly distributed along one edge of the aluminum plate while the other end of the laminate is constrained. The variations of radial and tangential stresses around the hole boundary in aluminum and composite plates are shown in Figs. 14 and 15, respectively. These figures demonstrate the capability of the two-dimensional analysis to capture the stress concentrations and provide the contact region around the bolt hole. The segment of the radial stresses with negative values establishes the contact region between the bolt and hole boundary. As expected, there are zero shear stresses on the hole boundary because of the absence of friction.

Based on the in-plane stress analysis, the maximum hole enlargements are computed as $\gamma_1^{(1)} = 6.808 \times 10^{-4}$ in and $\gamma_2^{(1)} = 2.891 \times 10^{-4}$ in for the aluminum and laminate, respectively. Invoking these values in Eq. (1), the stiffness of the spring representing the aluminum layer has a value of $k_{1,i}^{(1)} = 69,597$ lb/in with $i = 1,40$. The spring stiffness value for each ply of the laminate is

calculated as $k_{2,m}^{(1)} = 34,286$ lb/in, $k_{2,n}^{(1)} = 52,586$ lb/in, $k_{2,p}^{(1)} = 34,654$ lb/in, and $k_{2,q}^{(1)} = 8,446$ lb/in, where the subscripts *m*, *n*, *p*, and *q* represent 45°, 0°, -45°, and 90° plies, respectively.

The variation of the nodal displacements, $\Delta_{1,j}^{(1)}$ with $(j = 1,81)$ and $\Delta_{2,j}^{(1)}$ with $(j = 1,41)$, illustrates the bolt/hole deformations in Fig. 16. As observed in this figure, the deformations in the composite laminate are larger than those in the metal plate as dictated by the material properties and laminate thickness. As expected, the specified large values for head and nut rotational stiffness coefficients, k_h and k_n, result in zero slopes at the ends of the bolt. The maximum bolt/hole deformations occur at the interface of the two plates, indicating the location of the major load transfer, as reflected in Fig. 17, which depicts the variation of the load distribution through the thickness of the joint. As expected, the load distribution through the thickness of aluminum plate varies continuously. However, the ply loads corresponding to the composite laminate change abruptly, depending on the fiber orientation. This behavior is dictated by the material property discontinuity in the thickness direction resulting in a different stress state in each ply.

As presented in Table 2, the initial ply failure is predicted at a load level of $P = 3,656$ lbs, with a net-section failure mode in ply number 10 with a 90° fiber orientation. As the applied joint load is increased incrementally, the plies with a 90° fiber orientation continue failing in the net-section failure mode. Their failure is followed by a mixture of ±45° and 0° plies in the net-section and bearing failure modes, respectively. The load increments resulting in no failure have been omitted in Table 2.

At load increment 56, ply number 1 with a 45° fiber orientation ultimately fails at a load level of $P = 5,336$ lbs. This ply failure is followed by eleven different ply failures at the same load level. Therefore, the ultimate joint failure is reached at load increment 67 at a load level of 5,336 lbs. This prediction is in acceptable agreement with the experimental measurement of 4,910 lbs reported by Ramkumar et al.[2]

Three-Bolt Double-Lap Metal to Composite Joint

The geometrical parameters shown in Fig. 12 are defined by $W = 2.05$ in, $L_1 = 3.6$ in, $L_2 = 4.525$ in, $s_1 = 1.025$ in, $s_2 = 1.0$ in, $s_3 = 0.9$ in, $s_4 = 1.8$ in, $h_1 = 1.025$ in, $h_2 = 0.5$ in, $h_3 = 0.4$ in, and $d = 0.3125$ in. The initial joint load of $P = 205$ lbs is applied to the aluminum plate while the ends of the composite laminates are constrained. The maximum hole enlargement values associated with each bolt hole are computed from the two-dimensional analysis and are presented in Table 3, and the spring stiffness values for each ply are in Table 4.

The through-the-thickness variation of the ply loads near bolt number 3 is shown in Fig. 18. The corresponding bolt/hole deformations are depicted in Fig. 19. As observed in these figures, the most pronounced deformation occurs in plies located along the plate interfaces. Both deformations and ply load distributions are identical for composite laminates due to the presence of symmetry in the material and geometry.

Bolts 2 and 3 exert higher loads on the composite than bolt 1. The sequence ply failure loads and modes associated with each bolt are different because of the different strain states in the laminate near each bolt hole.

As presented in Table 5, the initial ply failure near bolt 1 occurs at a load level of 22,402 lbs, in ply number 19 with a 45° fiber orientation, in the shear-out failure mode. Part of the laminate near bolt 1 becomes unstable at load increment 23, corresponding to a load of 24,745 lbs, in ply 10 with a 90° fiber orientation, in the net-section ultimate failure. At this load level, seventeen more failures occur in the composite laminate before the laminate is assumed to ultimately fail at load increment 39.

As presented in Tables 6 and 7, the initial ply failures near bolts 2 and 3 occur at 13,124 lbs and 12,769 lbs, respectively, in ply 11 with a 90° fiber orientation, in the net-section failure mode. The progress of failure near bolt 2 is presented in Table 6. Starting at load increment 46 and until 64, failure occurs for nineteen increments in different plies at a load of 18,225 lbs, and the joint can still carry more load. Finally, ultimate failure of the joint occurs at load increment 69, corresponding to a load level of 19,155 lbs, in ply 2 with a 0° fiber orientation, in shear-out ultimate failure.

A similar failure behavior is observed near bolt 3, as presented in Table 7. At load increment 24, corresponding to a load of 13,965 lbs, failure occurs in ply 1 with a 45° fiber orientation, in the net-section failure mode, followed by fifteen failures in different plies at the same load level until ultimate joint failure.

Thus, the ultimate joint failure load is computed as 13,965 lbs near bolt 3. As shown in Table 7, the sequence of ply failure indicates that 90° and ±45° plies fail with the net-section failure mode while 0° plies fail with the shear-out failure mode.

Four-Bolt Single-Lap Metal to Composite Joint

The geometrical parameters for the four-bolt double-lap joint shown in Fig. 13 are defined by $W = 3.125$ in, $s = 1.25$ in, $e = 0.9375$ in, $\ell = 2.75$ in, and $D = 0.3125$ in.

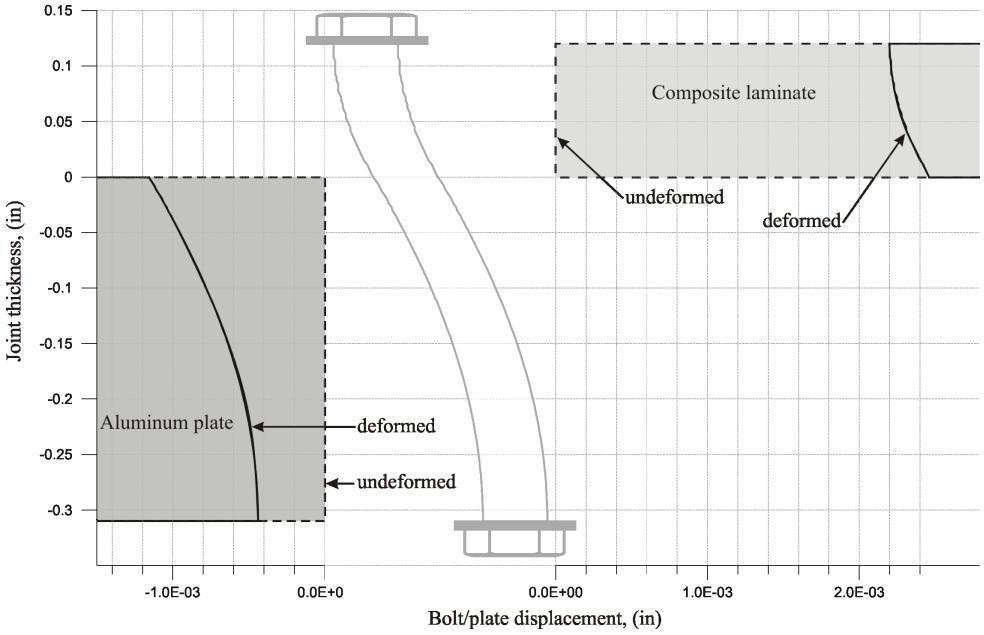

Fig. 16 Variation of bolt/plate displacement through the joint thickness.

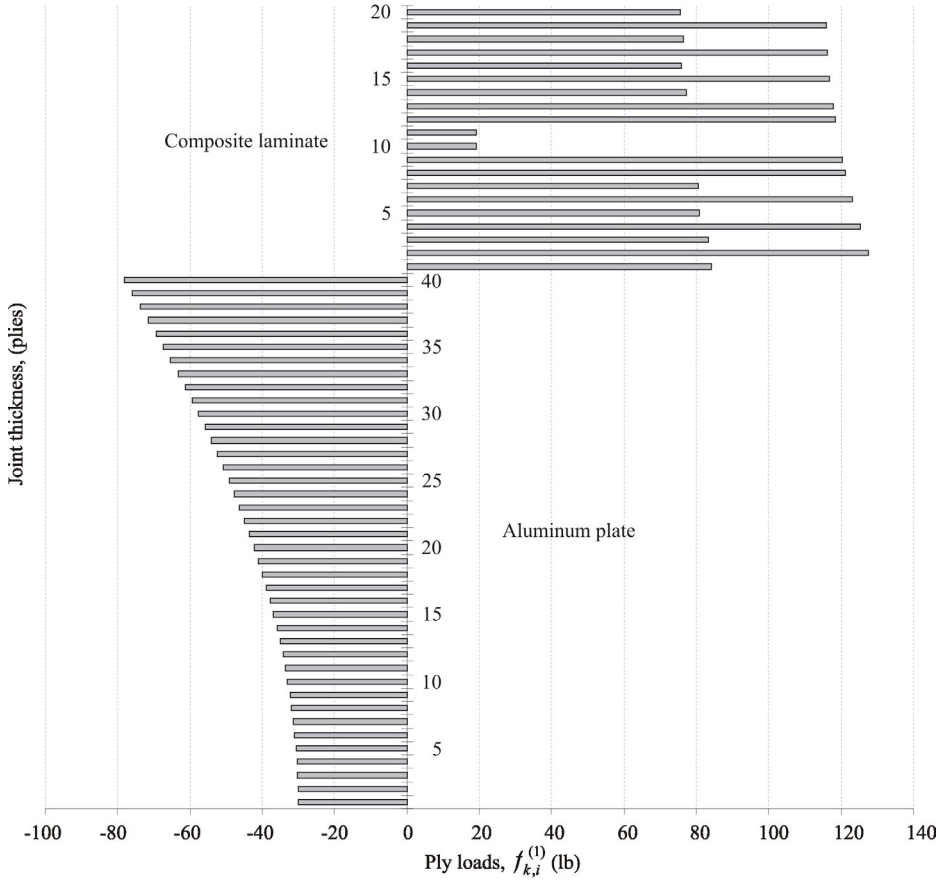

Fig. 17 Variation of ply loads through the joint thickness.

Table 2 Progressive ply failure in one-bolt single-lap joint.

Load increment	Applied joint load, (lb)	Ply number	Ply orientation, (degree)	Failure mode
1	3656	10	90	net-section
3	3693	11	90	net-section
19	4287	11	90	net-section ultimate
22	4373	10	90	net-section ultimate
34	4879	1	45	net-section
37	4977	3	-45	net-section
39	5027	5	45	net-section
41	5077	2	0	bearing
43	5128	4	0	bearing
44	5128	7	-45	net-section
46	5179	6	0	bearing
48	5231	8	0	bearing
50	5283	9	0	bearing
51	5283	14	-45	net-section
52	5283	16	45	net-section
53	5283	18	-45	net-section
54	5283	20	45	net-section
56	5336	1	45	net-section ultimate
57	5336	3	-45	net-section ultimate
58	5336	5	45	net-section ultimate
59	5336	7	-45	net-section ultimate
60	5336	12	0	bearing
61	5336	13	0	bearing
62	5336	14	-45	net-section ultimate
63	5336	15	0	bearing
64	5336	15	0	bearing ultimate
65	5336	12	0	bearing ultimate
66	5336	13	0	bearing ultimate
67	5336	16	45	net-section ultimate

Table 3 Maximum hole enlargement in a three-bolt double-lap joint.

	Bolt 1, (in)	Bolt 2, (in)	Bolt 3 (in)
Aluminum plate	4.068×10^{-5}	3.053×10^{-5}	3.174×10^{-5}
Composite plate	3.933×10^{-5}	5.723×10^{-5}	6.090×10^{-5}

\

Table 4 Spring stiffness values in a three-bolt double-lap joint.

		Bolt 1 (lb/in)	Bolt 2 (lb/in)	Bolt 3 (lb/in)
Aluminum plate		40,338	53,518	57,991
Plies in composite plate	45^0	29,071	22,589	28,862
	0^0	54,629	37,740	39,221
	-45^0	38,564	24,102	21,403
	90^0	9,043	5,832	6,433

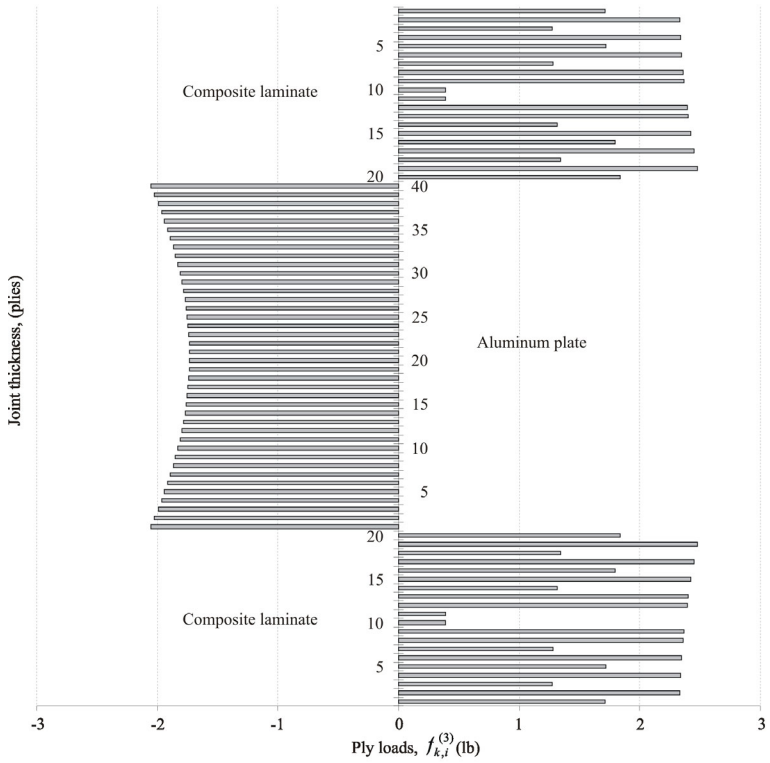

Fig. 18 Variation of ply loads through the joint thickness near bolt 3 in a three-bolt joint.

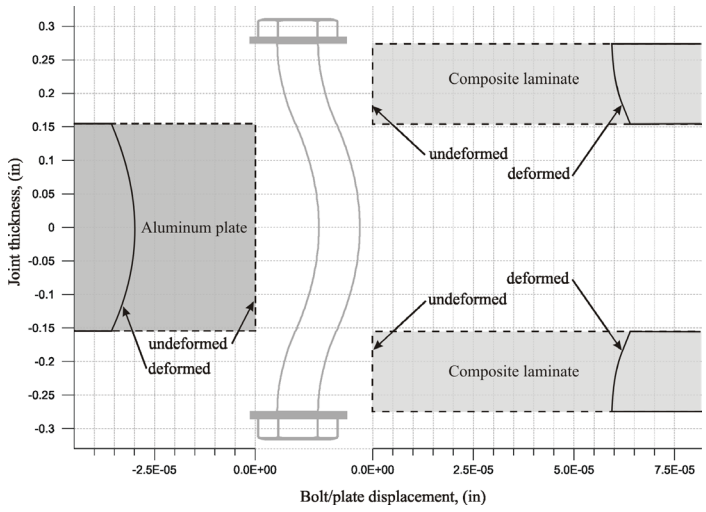

Fig. 19 Variation of bolt/plate displacement through the joint thickness near bolt 3 in a three-bolt joint.

Table 5 Progressive ply failure for bolt 1 in the three-bolt double-lap joint.

Load increment	Bolt load, (lb)	Applied joint load, (lb)	Ply number	Ply orientation, (degree)	Failure mode
1	3601	22402	19	0	shear-out
4	3673	22852	11	90	net-section
5	3673	22852	17	0	shear-out
7	3710	23080	10	90	net-section
8	3710	23080	15	0	shear-out
10	3747	23311	13	0	shear-out
12	3784	23544	12	0	shear-out
14	3822	23780	8	0	shear-out
15	3822	23780	9	0	shear-out
17	3860	24017	2	0	shear-out
18	3860	24017	4	0	shear-out
19	3860	24017	6	0	shear-out
23	3977	24745	10	90	net-section ultimate
24	3977	24745	14	-45	net-section
25	3977	24745	18	-45	net-section
26	3977	24745	18	-45	net-section ultimate
27	3977	24745	3	-45	net-section
28	3977	24745	3	-45	net-section ultimate
29	3977	24745	7	-45	net-section
30	3977	24745	7	-45	net-section ultimate
31	3977	24745	1	45	net-section
32	3977	24745	1	45	net-section ultimate
33	3977	24745	2	0	shear-out ultimate
34	3977	24745	4	0	shear-out ultimate
35	3977	24745	5	45	net-section
36	3977	24745	5	45	net-section ultimate
37	3977	24745	6	0	shear-out ultimate
38	3977	24745	8	0	shear-out ultimate
39	3977	24745	9	0	shear-out ultimate

Table 6 Progressive ply failure for bolt 2 in the three-bolt double-lap joint.

Load increment	Bolt load, (lb)	Applied joint load, (lb)	Ply number	Ply orientation, (degree)	Failure mode
1	2101	13124	11	90	net-section
3	2122	13255	10	90	net-section
17	2415	15086	10	90	net-section ultimate
22	2513	15698	11	90	net-section ultimate
26	2589	16174	18	-45	net-section
29	2641	16499	14	-45	net-section
31	2668	16664	20	45	net-section
33	2694	16831	7	-45	net-section
35	2721	16999	3	-45	net-section
36	2721	16999	16	45	net-section
40	2804	17514	1	45	net-section
41	2804	17514	5	45	net-section
46	2917	18225	18	-45	net-section ultimate
47	2917	18225	3	-45	net-section ultimate
48	2917	18225	5	45	net-section ultimate
49	2917	18225	1	45	net-section ultimate
50	2917	18225	7	-45	net-section ultimate
51	2917	18225	14	-45	net-section ultimate
52	2917	18225	16	45	net-section ultimate
53	2917	18225	12	0	shear-out
54	2917	18225	13	0	shear-out
55	2917	18225	15	0	shear-out
56	2917	18225	17	0	shear-out
57	2917	18225	19	0	shear-out
58	2917	18225	20	45	net-section ultimate
59	2917	18225	2	0	shear-out
60	2917	18225	4	0	shear-out
61	2917	18225	6	0	shear-out
62	2917	18225	8	0	shear-out
63	2917	18225	9	0	shear-out
69	3066	19155	2	0	shear-out ultimate

Table 7 Progressive ply failure for bolt 3 in the three-bolt double-lap joint.

Load increment	Bolt load, (lb)	Applied joint load, (lb)	Ply number	Ply orientation, (degree)	Failure mode
1	2302	12769	11	90	net-section
3	2325	12897	10	90	net-section
6	2372	13156	19	0	shear-out
8	2395	13288	17	0	shear-out
10	2419	13420	15	0	shear-out
11	2419	13420	20	45	net-section
13	2443	13555	12	0	shear-out
14	2443	13555	13	0	shear-out
16	2468	13690	6	0	shear-out
17	2468	13690	8	0	shear-out
18	2468	13690	9	0	shear-out
19	2468	13690	16	45	net-section
21	2493	13827	2	0	shear-out
22	2493	13827	4	0	shear-out
24	2517	13965	1	45	net-section
25	2517	13965	5	45	net-section
26	2517	13965	5	45	net-section ultimate
27	2517	13965	1	45	net-section ultimate
28	2517	13965	3	-45	net-section
29	2517	13965	7	-45	net-section
30	2517	13965	10	90	net-section ultimate
31	2517	13965	11	90	net-section ultimate
32	2517	13965	14	-45	net-section
33	2517	13965	14	-45	net-section ultimate
34	2517	13965	2	0	shear-out ultimate
35	2517	13965	3	-45	net-section ultimate
36	2517	13965	4	0	shear-out ultimate
37	2517	13965	6	0	shear-out ultimate
38	2517	13965	7	-45	net-section ultimate
39	2517	13965	8	0	shear-out ultimate

An initial joint load of $P = 312.5$ lbs is applied to the composite laminate while the end of the aluminum plate is constrained. Due to the presence of symmetry in geometry and loading, only the results concerning bolts 1 and 3 are presented. The maximum hole enlargement values associated with these bolt holes that were computed from the two-dimensional analysis are presented in Table 8, and the spring stiffness values for each ply are in Table 9.

The through-the-thickness variation of the ply loads near bolt number 1 is shown in Fig. 20. The corresponding bolt/hole deformations are depicted in Fig. 21. As observed in these figures, the most pronounced deformation occurs in plies located along the plate interfaces.

As presented in Table 10, the initial ply failure near bolt 3 occurs at a load level of 14,507 lbs, in ply number 1 with a 45° fiber orientation, in the net-section failure mode. The failure progresses with the ±45° and 90° fiber orientations in the net-section mode, and further continues with the failure of plies with 0° fiber orientation in the bearing mode. Part of the laminate near bolt 1 becomes unstable at load increment 50, corresponding to a load of 18,790 lbs, in ply 7 with a -45° fiber orientation, in the net-section failure. At this load level, seven more failures occur in the composite laminate before the laminate is assumed to ultimately fail at load increment 71, at a load level of 21,599 lbs. Near bolt 3, the initial ply initial failure occurs at 8,261 lbs, in ply 2 with 0° fiber orientation, in the shear-out failure mode as presented in Table 11. The failure progresses with plies of 0^0 fiber orientation in shear-out mode. Part of the laminate near bolt 3 becomes unstable at load increment 29, corresponding to a load of 9,401 lbs, in ply 3 with a -45° fiber orientation, in the net-section ultimate failure. At this load level, 11 more failures occur in the composite laminate before the laminate

Table 8 Maximum hole enlargement in the four-bolt single-lap joint.

	Bolt 1, (in)	Bolt 3, (in)
Aluminum plate	0.4144×10^{-4}	0.3169×10^{-4}
Composite plate	0.8532×10^{-4}	1.4378×10^{-4}

Table 9 Spring stiffness values in the four-bolt single-lap joint.

		Bolt 1, (lb/in)	Bolt 3, (lb/in)
Aluminum plate		39,527	63,183
Plies in composite plate	45^0	37,955	21,018
	0^0	51,811	38,542
	-45^0	34,835	29,017
	90^0	8,747	6,516

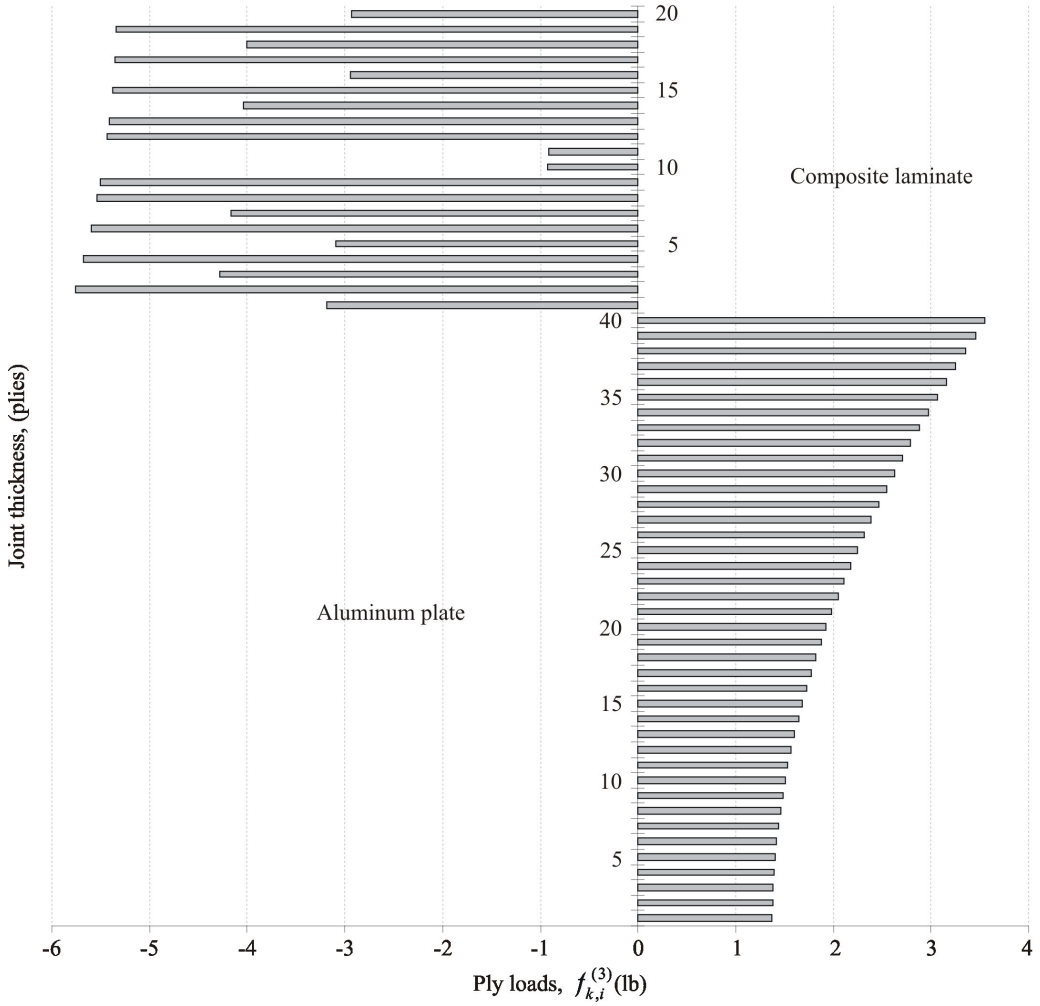

Fig. 20 Variation of ply loads through the joint thickness near bolt 3 in the four-bolt joint.

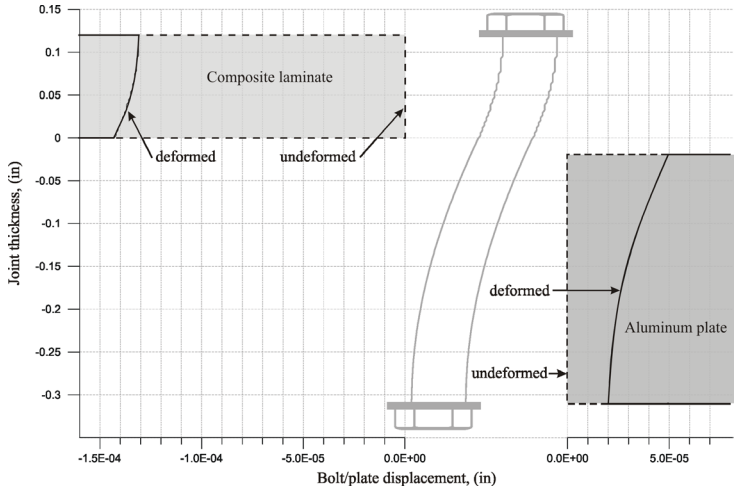

Fig. 21 Variation of bolt/plate displacement through the joint thickness near bolt 3 in the four-bolt joint.

Table 10 Progressive ply failure for bolt 1 in the four-bolt single-lap joint.

Load increment	Bolt load, (lb)	Applied joint load, (lb)	Ply number	Ply orientation, (degree)	Failure mode
1	3296	14507	1	45	net-section
6	3430	15096	5	45	net-section
14	3678	16185	16	45	net-section
15	3678	16185	20	45	net-section
20	3827	16842	10	90	net-section
21	3827	16842	11	90	net-section
24	3904	17181	1	45	net-section ultimate
25	3904	17181	5	45	net-section ultimate
26	3904	17181	10	90	net-section ultimate
27	3904	17181	16	45	net-section ultimate
28	3904	17181	11	90	net-section ultimate
29	3904	17181	20	45	net-section ultimate
32	3984	17526	2	0	bearing
34	4022	17701	4	0	bearing
37	4103	18057	6	0	bearing
39	4144	18238	8	0	bearing
40	4144	18238	9	0	bearing
42	4185	18420	3	-45	net-section
43	4185	18420	12	0	bearing
45	4227	18604	13	0	bearing
46	4227	18604	15	0	bearing
47	4227	18604	17	0	bearing
48	4227	18604	19	0	bearing
50	4270	18790	7	-45	net-section
51	4270	18790	7	-45	net-section ultimate
52	4270	18790	3	-45	net-section ultimate
53	4270	18790	14	-45	net-section
54	4270	18790	14	-45	net-section ultimate
55	4270	18790	18	-45	net-section
56	4270	18790	18	-45	net-section ultimate
71	4908	21599	2	0	bearing ultimate

Table 11 Progressive ply failure for bolt 3 in the four-bolt single-lap joint.

Load increment	Bolt load, (lb)	Applied joint load, (lb)	Ply number	Ply orientation, (degree)	Failure mode
1	2260	8261	2	0	shear-out
4	2305	8427	4	0	shear-out
6	2329	8511	6	0	shear-out
8	2352	8596	8	0	shear-out
10	2375	8682	9	0	shear-out
12	2399	8769	12	0	shear-out
13	2399	8769	13	0	shear-out
14	2399	8769	15	0	shear-out
16	2423	8857	10	90	net-section
17	2423	8857	17	0	shear-out
18	2423	8857	19	0	shear-out
20	2447	8945	11	90	net-section
21	2447	8945	11	90	net-section ultimate
25	2521	9216	3	-45	net-section
27	2547	9308	7	-45	net-section
29	2572	9402	3	-45	net-section ultimate
30	2572	9402	7	-45	net-section ultimate
31	2572	9402	10	90	net-section ultimate
32	2572	9402	14	-45	net-section
33	2572	9402	14	-45	net-section ultimate
34	2572	9402	1	45	net-section
35	2572	9402	1	45	net-section ultimate
36	2572	9402	2	0	shear-out ultimate
37	2572	9402	4	0	shear-out ultimate
38	2572	9402	5	45	net-section
39	2572	9402	5	45	net-section ultimate
40	2572	9402	6	0	shear-out ultimate
41	2572	9402	8	0	shear-out ultimate

is assumed to ultimately fail at load increment 41. Thus, the ultimate joint failure load occurs near bolt 3 at a load level of 9,402 lbs.

Conclusions

In this study, an approach to predict the strength of single- and double-lap bolted composites has been developed based on the through-the-thickness ply loads of the laminate in conjunction with the average stress failure criterion. This approach utilizes the model of a beam on an elastic foundation to compute the corrected ply loads utilizing a two- dimensional stress analysis based on the complex potential and variational formulation. In the case of a one-bolt single-lap aluminum-to-composite joint, the joint strength prediction from the present approach is in acceptable agreement with the experimental measurement published previously. This approach proves that the ply load distribution in a laminate is significantly influenced near the bolt by the bolt bending deformations. This distribution is dependent on the plate thickness and laminate lay-up, and it is different for single- and double-lap bolted joints.

References

[1]Kradinov, V., Barut, A., Madenci, E., and Ambur, D. R., "Bolted Double-Lap Composite Joints Under Mechanical and Thermal Loading," *International Journal of Solids and Structures*, Vol. 38, 2001, pp. 57-75.

[2]Ramkumar, R. L., and Saether, E. S., "Strength Analysis of Composite and Metallic Plates Bolted Together by a Single Fastener," Aircraft Division, Report AFWAL-TR-85-3064, Northrop Corporation, Hawthorne, CA, August 1985.

[3]Whitney, J. M. and Nuismer, R. J., "Stress Fracture Criteria for Laminated Composites Containing Stress Concentrations," *Journal of Composite Materials*, Vol. 8, 1974, pp. 253-265.

[4]Kradinov, V., Madenci, E., and Ambur, D. R., "Analysis of Bolted Laminates of Varying Thickness and Lay-up with Metallic Inserts," AIAA Paper 2003-1998, April 2003.

[5]Eriksson, I., Backlund, J., and Moller, P., "Design of Multiple-Row Bolted Composite Joints Under General In-Plane Loading," *Composites Engineering*, Vol.5, 1995, pp. 1051-1068.

[6]Xiong Y., "An Analytical Method for Failure Pre diction of Multi-Fastener Composite Joints," *International Journal of Solids and Structures*, Vol. 33, 1995, pp. 4395-4409.

[7]Ghali, A., and Neville, A. M., *Structural Analysis: A Unified Classical and Matrix Approach*, Chapman and Hall, New York, 1978.

Appendix

In the k^{th} laminate, the strain energy of the l^{th} bolt, which is defined by a uniform cross-section, $A^{(\ell)}$, moment of inertia, $I^{(\ell)}$, and Young's and shear moduli, $E^{(\ell)}$ and $G^{(\ell)}$, respectively, can be expressed as

$$B_k^{(\ell)} = \sum_{i=1}^{K-1} \frac{1}{2} \mathbf{q}_k^{(i\ell)T} \mathbf{b}_k^{(i\ell)} \mathbf{q}_k^{(i\ell)} \tag{A1}$$

where $\mathbf{q}_k^{(i\ell)}$ represents the vector of nodal deflections and rotations for the i^{th} beam element and K is the number of nodes in the bolt discretization. The stiffness matrix for a two-node Timoshenko beam element is given by Ghali and Neville[7] as

$$\mathbf{b}_k^{(i\ell)} = \frac{1}{1+\alpha_k^{(il)}} \begin{bmatrix} \dfrac{12E^{(l)}I^{(l)}}{\left(h_k^{(il)}\right)^3} & & & \textbf{symmetric} \\ \dfrac{6E^{(l)}I^{(l)}}{\left(h_k^{(il)}\right)^2} & \left(4+\alpha_k^{(il)}\right)\dfrac{E^{(l)}I^{(l)}}{h_k^{(il)}} & & \\ -\dfrac{12E^{(l)}I^{(l)}}{\left(h_k^{(il)}\right)^3} & -\dfrac{6E^{(l)}I^{(l)}}{\left(h_k^{(il)}\right)^2} & \dfrac{12E^{(l)}I^{(l)}}{\left(h_k^{(il)}\right)^3} & \\ \dfrac{6E^{(l)}I^{(l)}}{\left(h_k^{(il)}\right)^2} & \left(2-\alpha_k^{(il)}\right)\dfrac{E^{(l)}I^{(l)}}{h_k^{(il)}} & -\dfrac{6E^{(l)}I^{(l)}}{\left(h_k^{(il)}\right)^2} & \left(4+\alpha_k^{(il)}\right)\dfrac{E^{(l)}I^{(l)}}{h_k^{(il)}} \end{bmatrix} \tag{A2}$$

where $\alpha_k^{(i\ell)} = (h_k^{(i\ell)})^2 G^{(\ell)} A^{(\ell)} / 12E^{(\ell)} I^{(\ell)} c$ in which c represents the shear correction factor.

Rearranging the right-hand side of Eq. (A1) such that the matrices are suitable for static condensation of the internal nodal rotations leads to

$$B_k^{(\ell)} = \frac{1}{2} \begin{Bmatrix} \boldsymbol{\Delta}_k^{(\ell)} \\ \mathbf{q}_{k,\phi}^{(\ell)} \end{Bmatrix}^T \begin{bmatrix} \mathbf{b}_{k,\Delta\Delta}^{(\ell)} & \mathbf{b}_{k,\Delta\phi}^{(\ell)} \\ \mathbf{b}_{k,\Delta\phi}^{(\ell)T} & \mathbf{b}_{k,\phi\phi}^{(\ell)} \end{bmatrix} \begin{Bmatrix} \boldsymbol{\Delta}_k^{(\ell)} \\ \mathbf{q}_{k,\phi}^{(\ell)} \end{Bmatrix} \tag{A3}$$

where

$$\begin{aligned} \boldsymbol{\Delta}_k^{(\ell)T} &= \left\{ \Delta_{k,1}^{(\ell)} \quad \phi_{k,1}^{(\ell)} \quad \Delta_{k,2}^{(\ell)} \quad \Delta_{k,3}^{(\ell)} \quad \cdots \quad \Delta_{k,K-1}^{(\ell)} \quad \Delta_{k,K}^{(\ell)} \quad \phi_{k,K}^{(\ell)} \right\} \\ \mathbf{q}_{k,\phi}^{(\ell)T} &= \left\{ \phi_{k,2}^{(\ell)} \quad \phi_{k,3}^{(\ell)} \quad \cdots \quad \phi_{k,(K-1)}^{(\ell)} \right\} \end{aligned} \tag{A4}$$

$$\mathbf{b}_{k,\Delta\Delta}^{(\ell)} = \begin{bmatrix} b_{k,11}^{(1\ell)} & b_{k,13}^{(1\ell)} & b_{k,12}^{(1\ell)} & & & & \\ b_{k,13}^{(1\ell)} & b_{k,33}^{(1\ell)} & b_{k,23}^{(1\ell)} & & & & \\ b_{k,12}^{(1\ell)} & b_{k,23}^{(1\ell)} & b_{k,22}^{(1\ell)} + b_{k,11}^{(2\ell)} & b_{k,12}^{(2\ell)} & & & \\ & & \ddots & \ddots & \ddots & \ddots & \\ & & & b_{k,12}^{((K-2)\ell)} & b_{k,22}^{((K-2)\ell)} + b_{k,11}^{((K-1)\ell)} & b_{k,12}^{((K-1)\ell)} & b_{k,14}^{((K-1)\ell)} \\ & & & & b_{k,12}^{((K-1)\ell)} & b_{k,22}^{((K-1)\ell)} & b_{k,24}^{((K-1)\ell)} \\ & & & & b_{k,14}^{((K-1)\ell)} & b_{k,24}^{((K-1)\ell)} & b_{k,44}^{((K-1)\ell)} \end{bmatrix} \tag{A5}$$

$$\mathbf{b}_{k,\Delta\phi}^{(\ell)} = \begin{bmatrix} b_{k,14}^{(1\ell)} & & & & \\ b_{k,34}^{(1\ell)} & & & & \\ b_{k,24}^{(1\ell)} + b_{k,13}^{(2\ell)} & b_{k,14}^{(2\ell)} & & & \\ b_{k,23}^{(2\ell)} & b_{k,24}^{(2\ell)} + b_{k,13}^{(3\ell)} & b_{k,14}^{(3\ell)} & & \\ & \ddots & \ddots & \ddots & \\ & & b_{k,23}^{((K-3)\ell)} & b_{k,24}^{((K-3)\ell)} + b_{k,13}^{((K-2)\ell)} & b_{k,14}^{((K-2)\ell)} \\ & & & b_{k,23}^{((K-2)\ell)} & b_{k,24}^{((K-2)\ell)} + b_{k,13}^{((K-1)\ell)} \\ & & & & b_{k,23}^{((K-1)\ell)} \\ & & & & b_{k,34}^{((K-1)\ell)} \end{bmatrix} \tag{A6}$$

$$\mathbf{b}_{k,\phi\phi}^{(\ell)} = \begin{bmatrix} b_{k,44}^{(1\ell)} + b_{k,33}^{(2\ell)} & b_{k,34}^{(2\ell)} & & & \\ b_{k,34}^{(2\ell)} & b_{k,44}^{(2\ell)} + b_{k,33}^{(3\ell)} & b_{k,34}^{(3\ell)} & & \\ & \ddots & \ddots & \ddots & \\ & & b_{k,34}^{((K-3)\ell)} & b_{k,44}^{((K-3)\ell)} + b_{k,33}^{((K-2)\ell)} & b_{k,34}^{((K-2)\ell)} \\ & & & b_{k,34}^{((K-2)\ell)} & b_{k,44}^{((K-2)\ell)} + b_{k,33}^{((K-1)\ell)} \end{bmatrix} \tag{A7}$$

Since the internal nodes are not subjected to external moments, the first variation of the strain energy with respect to the vector $\mathbf{q}_{k,\phi}^{(\ell)}$ vanishes, resulting in the moment equilibrium equations as

$$\mathbf{b}_{k,\Delta\phi}^{(\ell)\ T}\boldsymbol{\Delta}_k^{(\ell)} + \mathbf{b}_{k,\phi\phi}^{(\ell)}\mathbf{q}_{k,\phi}^{(\ell)} = \mathbf{0} \tag{A8}$$

Solving for $\mathbf{q}_{k,\phi}^{(\ell)}$ in the Eq. (A8) and substituting into Eq. (A3), after rearranging the terms, leads to

$$B_k^{(\ell)} = \frac{1}{2}\boldsymbol{\Delta}_k^{(\ell)T}\mathbf{b}_k^{(\ell)}\boldsymbol{\Delta}_k^{(\ell)} \tag{A9}$$

where the matrix $\mathbf{b}_k^{(\ell)}$ is defined as

$$\mathbf{b}_k^{(\ell)} = \mathbf{b}_{k,\Delta\Delta}^{(\ell)} - \frac{1}{2}\mathbf{b}_{k,\Delta\phi}^{(\ell)\ T}\mathbf{b}_{k,\phi\phi}^{(\ell)\ -1}\mathbf{b}_{k,\Delta\phi}^{(\ell)} \tag{A10}$$

The strain energy of the translational and rotational spring elements can be expressed as

$$S_k^{(\ell)} = \frac{1}{2}\overline{\boldsymbol{\Delta}}_k^{(\ell)T}\overline{\boldsymbol{k}}_k^{(\ell)}\overline{\boldsymbol{\Delta}}_k^{(\ell)} \tag{A11}$$

in which $\overline{\boldsymbol{\Delta}}_k^{(\ell)}$ is the same as $\boldsymbol{\Delta}_k^{(\ell)}$ with an additional degree of freedom representing the rigid base for the springs, and $\overline{\boldsymbol{k}}_k^{(\ell)}$ is defined as

$$\overline{\boldsymbol{k}}_k^{(\ell)} = \begin{bmatrix} & & & & & & & & & & & & \\ & & & & & & & & & & & & -k_{k,h}^{(\ell)} \\ & & k_{k,1}^{(\ell)} & & & & & & & & & & -k_{k,1}^{(\ell)} \\ & & & & & & & & & & & & \\ & & & & k_{k,2}^{(\ell)} & & & & & & & & -k_{k,2}^{(\ell)} \\ & & & & & \ddots & & & & & & & \\ & & & & & & k_{k,N_k-1}^{(\ell)} & & & & & & -k_{k,N_k-1}^{(\ell)} \\ & & & & & & & & & & & & \\ & & & & & & & & k_{k,N_k}^{(\ell)} & & & & -k_{k,N_k}^{(\ell)} \\ & & & & & & & & & & & & \\ & & & & & & & & & & k_{k,n}^{(\ell)} & & \\ & -k_{k,h}^{(\ell)} & -k_{k,1}^{(\ell)} & & -k_{k,2}^{(\ell)} & & -k_{k,N_k-1}^{(\ell)} & & -k_{k,N_k}^{(\ell)} & & & \sum_{i=1}^{N_k} k_{k,i}^{(\ell)} \end{bmatrix} \tag{A12}$$

where the last column and row appear due to degrees of freedom associated with the rigid base. Since the rigid base is fixed, this column and row are eliminated from the matrix in Eq. (A12). Thus, the total strain energy of the beam on an elastic foundation can be written as

$$U_k^{(\ell)} = B_k^{(\ell)} + S_k^{(\ell)} \tag{A13a}$$

or

$$U_k^{(\ell)} = \frac{1}{2}\boldsymbol{\Delta}_k^{(\ell)T}\left(\mathbf{b}_k^{(\ell)} + \boldsymbol{k}_k^{(\ell)}\right)\boldsymbol{\Delta}_k^{(\ell)} \tag{A13b}$$

in which $\boldsymbol{k}_k^{(\ell)}$ is defined by

$$\boldsymbol{k}_k^{(\ell)} = \begin{bmatrix} 0 & & & & & & & & & & & \\ & k_{k,h}^{(\ell)} & & & & & & & & & & \\ & & k_{k,1}^{(\ell)} & & & & & & & & & \\ & & & 0 & & & & & & & & \\ & & & & k_{k,2}^{(\ell)} & & & & & & & \\ & & & & & \ddots & & & & & & \\ & & & & & & k_{k,N_k-1}^{(\ell)} & & & & & \\ & & & & & & & 0 & & & & \\ & & & & & & & & k_{k,N_k}^{(\ell)} & & & \\ & & & & & & & & & 0 & & \\ & & & & & & & & & & k_{k,n}^{(\ell)} & \end{bmatrix} \tag{A14}$$

In the case of a single-lap bolted joint, the bolt nut is not present in the top plate, k =1, while the bolt head is not present in the bottom plate, k =2; thus, $k_{1,n}^{(\ell)} = 0$ in the top plate and $k_{2,h}^{(\ell)} = 0$ in the bottom plate. In the absence of both head and nut in the middle plate of a double-lap bolted joint, in addition to the values of $k_{1,n}^{(\ell)} = k_{3,h}^{(\ell)} = 0$ for the top and bottom plates, $k_{2,h}^{(\ell)} = k_{2,n}^{(\ell)} = 0$ in the middle plate.

The total potential energy of the ℓ^{th} bolt can be expressed as

$$\pi = U^{(\ell)} - W^{(\ell)} = \frac{1}{2}\boldsymbol{\Delta}^{(\ell)T}\mathbf{K}^{(\ell)}\boldsymbol{\Delta}^{(\ell)} - \mathbf{F}\boldsymbol{\Delta}^{(\ell)} \tag{A15}$$

where

$$\mathbf{K}^{(\ell)} = \begin{bmatrix} \mathbf{b}_1^{(\ell)} + \mathbf{k}_1^{(\ell)} & \mathbf{0} \\ \mathbf{0} & \mathbf{b}_2^{(\ell)} + \mathbf{k}_2^{(\ell)} \end{bmatrix}, \qquad \mathbf{F} = \begin{bmatrix} 0 \\ \vdots \\ 0 \\ P_1^{(\ell)} \\ P_2^{(\ell)} \\ 0 \\ \vdots \\ 0 \end{bmatrix} \begin{matrix} \\ \\ \\ \text{node } K \\ \text{node } K+1 \\ \\ \\ \\ \end{matrix}$$

and

$$\boldsymbol{\Delta}^{(\ell)T} = \left\{ \Delta_1^{(\ell)} \quad \phi_1^{(\ell)} \quad \Delta_2^{(\ell)} \quad \cdots \quad \Delta_{K+M}^{(\ell)} \quad \phi_{K+M}^{(\ell)} \right\}$$

for a single-lap joint, and

$$\mathbf{K}^{(\ell)} = \begin{bmatrix} \mathbf{b}_1^{(\ell)} + \mathbf{k}_1^{(\ell)} & \mathbf{0} & \mathbf{0} \\ \mathbf{0} & \mathbf{b}_2^{(\ell)} + \mathbf{k}_2^{(\ell)} & \mathbf{0} \\ \mathbf{0} & \mathbf{0} & \mathbf{b}_3^{(\ell)} + \mathbf{k}_3^{(\ell)} \end{bmatrix}, \qquad \mathbf{F} = \begin{bmatrix} 0 \\ \vdots \\ 0 \\ P_1^{(\ell)} \\ -P_1^{(\ell)} \\ 0 \\ \vdots \\ 0 \\ P_1^{(\ell)} + P_2^{(\ell)} = -P_3^{(\ell)} \\ P_3^{(\ell)} \\ 0 \\ \vdots \\ 0 \end{bmatrix} \begin{matrix} \\ \\ \\ \\ \\ \text{node } K \\ \text{node } K+1 \\ \\ \text{node } K+M \\ \text{node } K+M+1 \\ \\ \\ \end{matrix} \tag{A16}$$

and

$$\boldsymbol{\Delta}^{(\ell)T} = \left\{ \Delta_1^{(\ell)} \quad \phi_1^{(\ell)} \quad \Delta_2^{(\ell)} \quad \cdots \quad \Delta_{K+M}^{(\ell)} \quad \phi_{K+M}^{(\ell)} \quad \cdots \quad \Delta_{K+M+P}^{(\ell)} \quad \phi_{K+M+P}^{(\ell)} \right\} \tag{A17}$$

for a double-lap joint. The variables K, M, and P define the number of nodes in the beam discretization for each plate.

According to the bilinear behavior of the ply loads shown in Fig. 10, the coefficients of the matrix $\boldsymbol{k}_k^{(\ell)}$ become $\hat{k}_{k,i}^{(\ell)}$ [$\hat{k}_{k,i}^{(\ell)} = \alpha k_{k,i}^{(\ell)}$, where $\alpha = 0.1$] for initially damaged plies and zero for totally damaged plies. Also, for initially damaged plies, the values of $(k_{k,i}^{(\ell)} - \hat{k}_{k,i}^{(\ell)})\Delta_{k,j}^{(\ell)IN}$ are added to the corresponding locations in the vector of externally applied loads, $\mathbf{F}$.

Appling the principle of minimum potential energy and forcing the first variation of the total potential to vanish, $\delta\pi = 0$, leads to the system of equilibrium equations

$$\mathbf{K}^{(\ell)}\boldsymbol{\Delta}^{(\ell)} = \mathbf{F}^{(\ell)} \tag{A19}$$

In the finite element formulation of the problem, additional constraint equations are introduced to ensure the continuity of the rotational degree of freedom between the adjacent section of the beam

$$\begin{cases} \phi_K^{(\ell)} = \phi_{K+1}^{(\ell)} & \text{for a single lap joint} \\ \begin{cases} \phi_K^{(\ell)} = \phi_{K+1}^{(\ell)} \\ \phi_{K+M}^{(\ell)} = \phi_{K+M+1}^{(\ell)} \end{cases} & \text{for a double lap joint} \end{cases} \tag{A20}$$

These constraint conditions are enforced by adding an additional row and column with all but two elements set to zero in the matrix $\mathbf{K}^{(\ell)}$. Two nonzero elements are set to 1 and -1 in the locations corresponding to the nodal rotations; a zero value is added in the right-hand side.

#